frontiers | Frontiers in Earth Science

TYPE Original Research
PUBLISHED 12 January 2023
DOI 10.3389/feart.2022.1035655

OPEN ACCESS

EDITED BY
Lupeng Yu,
Linyi University, China

REVIEWED BY
Xiaomei Nian,
East China Normal University, China
Fei Han,
Yunnan University, China

*CORRESPONDENCE
Gongming Yin,
yingongming@ies.ac.cn

†These authors share first authorship

SPECIALTY SECTION
This article was submitted to Quaternary Science, Geomorphology and Paleoenvironment,
a section of the journal
Frontiers in Earth Science

RECEIVED 03 September 2022
ACCEPTED 31 October 2022
PUBLISHED 12 January 2023

CITATION
Wei C, Yin G, Du J, Liu C, Cheng L, Ji H and Wang L (2023), Residual electron spin resonance signals of quartz from the 2018 Baige dammed lake in Tibet: Implications for the identification of sediment layers caused by megafloods. *Front. Earth Sci.* 10:1035655.
doi: 10.3389/feart.2022.1035655

Residual electron spin resonance signals of quartz from the 2018 Baige dammed lake in Tibet: Implications for the identification of sediment layers caused by megafloods

Chuanyi Wei[1†], Gongming Yin[1*], Jinhua Du[2], Chunru Liu[1], Li Cheng[1,3], Hao Ji[1] and Libin Wang[1]

[1]State Key Laboratory of Earthquake Dynamics, Institute of Geology, China Earthquake Administration, Beijing, China, [2]School of Earth Science and Resources, Chang'an University, Xi'an, China, [3]China Earthquake Disaster Prevention Center, China Earthquake Administration, Beijing, China

Residual doses may cause overestimation of electron spin resonance (ESR) ages for fluvial sediments. However, ESR residual doses in outburst megaflood sediments have rarely been evaluated. The Jinsha River, situated in the southeastern Tibetan Plateau, is characterized by active faults, narrowed canyons, and dammed lakes. Consequently, the river is a rare opportunity for a reconstruction study of outburst flood events from a paleo-dammed lake. After the destruction of the Baige dammed lake in the upper Jinsha River in 2018, outburst megafloods formed a thick diluvium that was deposited in broad valley land along the lower Jinsha River. Based on detailed field investigation and laboratory studies, preliminary hydraulics estimates and residual quartz ESR signals indicate the following. 1) Among the multiple quartz ESR centers, the Al, E_1', Ti-H, and Ti-Li centers could be measured. The Ti-H center had the lowest residual dose and would provide relatively accurate ages for outburst megaflood sediment. 2) The Ti-Li and Al centers commonly used for ESR dating provide overestimates of 283 ± 42 ka ~ 462 ± 63 ka and 1,010 ± 88 ka ~ 1,400 ± 219 ka, respectively, for present outburst megaflood sediment. 3) The diverse ages given by the same ESR signal may be caused by various precursors of megaflood sediments, which are mainly sourced from landslide dams and from various terraces and slope sediments along the river. Results demonstrated that the apparent ESR ages observed for the outburst megaflood sediment in the southeastern Tibetan Plateau may be counterfeit, providing an age much older than its real age. This could be interpreted to mean that the narrowed lower channel makes the upper reaches of the broad valley appear lake-like, with diluvium deposits having large non-negligible residual ESR signals without enough exposure to adequate sunlight, despite having good stratification and sorting characteristics similar to those of fluvio-lacustrine sediments. Thus, abrupt reversal in quartz ESR ages in multiple centers observed in the geochronological framework of the fluvial

sedimentary profile may indicate a diluvial or flood layer in the absence of other inducements.

KEYWORDS

Tibetan plateau, canyon area, dammed lake, outburst megaflood sediment, electron spin resonance

Highlights

- Outburst megaflood sediments induced by destruction of a dammed lake show good stratification and sorting characteristics.
- Quartz ESR signals of megaflood sediments are rarely bleached prior to burial.
- Various precursors of megaflood sediments contribute to large ESR D_e values.
- Abrupt reversal of ESR age may indicate megaflood sediment layers in fluvial sediment.

1 Introduction

The disastrous effects of megafloods caused by outbursts of dammed lakes on the geological environment have attracted the attention of environmental geologists, geomorphologists, and archeologists since the M_S 8.0 Wenchuan earthquake in China on 12 May 2008 because these can be severe enough to cause the disappearance of societies (Carrivick et al., 2011; Li et al., 2014; Wu et al., 2016; Dong et al., 2018; Li et al., 2020; Ding et al., 2021; Wang et al., 2021). Recently, the need for scientific information about megaflood deposits—in terms of their composition of materials, grain size distributions, sedimentary structure characteristics, and geochronology—has attained critical attention (Liu et al., 2019; Su et al., 2021).

Electron spin resonance (ESR) dating has been widely used to determine the geochronology of quaternary unconsolidated sediments (Grün, 1989; Rink, 1997; Voinchet et al., 2007, 2015, 2019; Duval et al., 2017; Voinchet et al., 2020; Wei et al., 2020). The evaluation of the resetting degree of ESR is essential, especially for the dating of rapidly accumulated deposits (Richter and Tsukamoto, 2022). Residual equivalent dose (D_e) values for ESR signals have been investigated using natural-sunlight optical bleaching (Voinchet et al., 2007; Gao et al., 2009; Gliganic et al., 2017), artificial sunlight simulation (Toyoda et al., 2000; Voinchet et al., 2003, 2017; Wei et al., 2018, 2019), and tumbler experiments (Liu and Grün, 2011). Previous studies have shown that ESR signals of modern fluvial (Voinchet et al., 2015; Tsukamoto et al., 2017) and alluvial sediments (Moreno et al., 2012; Cunningham et al., 2015; Bartz et al., 2020) can become zero or reach steady residual values before burial. However, the evaluation of the residual D_e value of the diluvium, especially that discharged from dammed lakes in the canyon area, has been rare.

In December 2018, a modern dam-breaching event occurred on the southeastern Tibetan Plateau (Figure 1), resulting in an outburst flood and the accumulation of thick outburst flood sediments downstream (Figure 2). In this study, field investigations and laboratory grain size experiments were performed for sedimentary texture analysis. Samples of these outburst flood sediments from different downstream river locations were obtained for ESR measurement in order to estimate residual doses in their quartz grains. This article discusses the implications of residual doses in recognizing the geo-historical fluvial profiles of paleo-megaflood layers.

2 The 2018 Baige dammed lake

The Baige area of the southeastern Tibetan Plateau has steep hills and valleys, severe landform incisions, and broken rocks (Guo et al., 2021). Before the 20th century, several strong earthquakes occurred around the Baige area, including the 1989 M_w 6.5 Batang earthquake, the 1870 M_w 7.2 Batang earthquake, and the 1842 M_w 7.3 Zongguo earthquake (SSB, 1995; Ambraseys and Douglas, 2004). Recently, the 2013 M_S 6.1 Changdu earthquake occurred in this area, resulting in 37 and 57 new potential hazards in Jiangda and Baiyu counties, respectively (Wang et al., 2019). These earthquakes intensified the frequency of landslide occurrence, including the Baige landslide.

2.1 Landslides and the creation of the Baige dammed lake

Due to the combination of heavy rainfall and long-term gravity movement, the Baige landslide occurred on 11 October 2018, blocking the Jinsha River and forming the Baige dammed lake in the southeastern Tibetan Plateau (Figure 1B; Guo et al., 2021). The landslide occurred on the right bank of the Jinsha River. The material moved by the landslide had a volume of approximately 2.5 million m^3, with an average accumulation height of 40 m above the channel bottom of the river (Guo et al., 2021). Water flowed into the dammed lake at approximately 1,700 m^3/s, accumulating approximately 0.15 billion m^3 of water in under 24 h (data

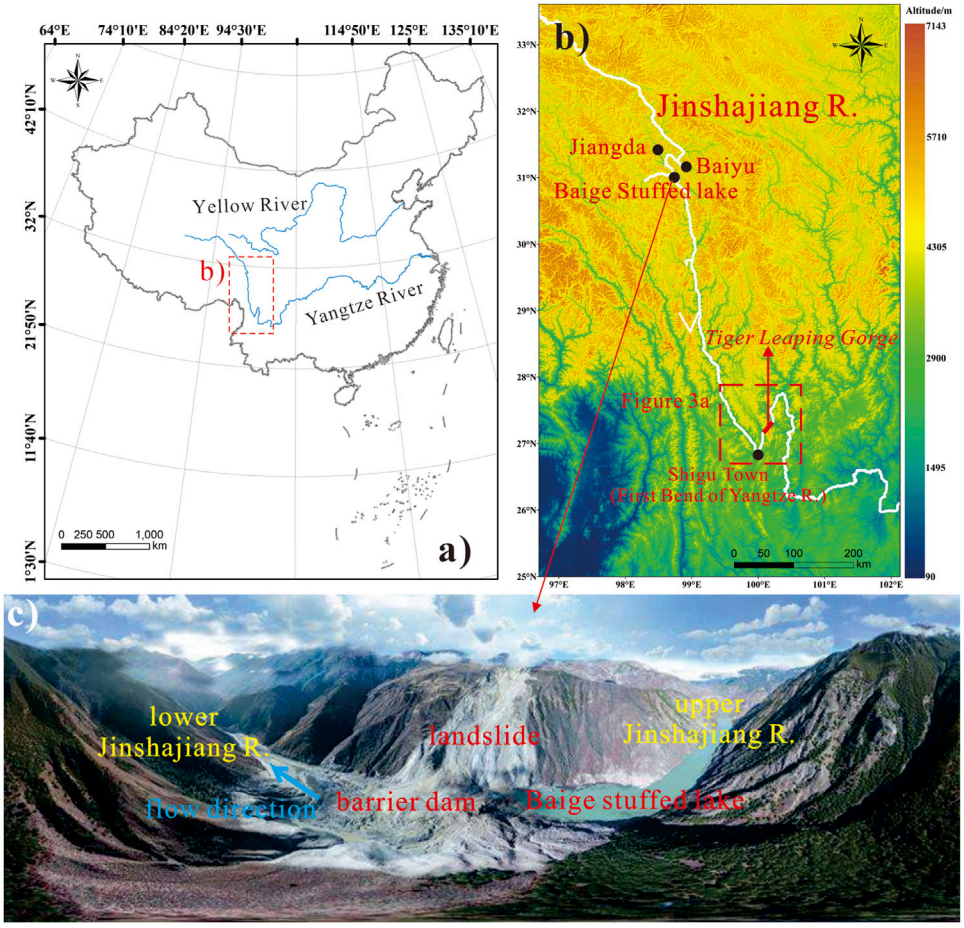

FIGURE 1
(A,B) Maps showing the location of the Jinsha River and the studied area. **(C)** Photograph of the Baige landslide dam (98° 42′ 17.98″ E and 31° 4′ 56.41″ N). Note that the picture was taken approximately 23 h after the landslide occurred, at 16:00 h on 5 November 2018.

from Changjiang Water Resources Commission). The maximum storage of the dammed lake (~0.3 billion m^3) was reached on the afternoon of 12 October 2018. The resulting dammed lake has a length of 2 km and a width ranging between 450 and 700 m (Guo et al., 2021). As the water naturally flowed downstream, the water level of the dammed lake dropped from 2,915.12 m to 2,894.60 m.

A second landslide occurred at the same place on the Jinsha River at 17:00 h on 3 November 2018. The volume of earth moved was ~2 million m^3, and the accumulated volume of earth was ~5 million m^3. The dammed lake has a length of ~270 m and a width of ~580 m. The elevation changed to ~2,970 m, which is 36 m higher than that of the first dammed lake. The estimated volume of the dammed lake is approximately 0.77 billion m^3. The Jinsha River was cut off by the dammed lake (Figures 1, 3; data from Changjiang Water Resources Commission).

2.2 Diluvium from the Baige dammed lake

After manual intervention, the flood caused by the destruction of the dammed lake entered the Shigu area (First Bend of the Yangtze River) at approximately 22:30 h on 14 November 2018. The highest flood level was 1,826.33 m, which was 3.80 m and 8.98 m higher than the warning (Figures 2, 3, 4) and normal water levels, respectively. The highest water flow rate was 7,070 m^3/s. The water level did not fall back to the normal level until 17:00 h on 15 November 2018. The relatively high water level lasted approximately 18 h in the First Bend area (Figure 3).

The rapidly narrowed TLG acted like a dam, preventing outburst floods from discharging downward quickly. This resulted in a momentary lake and caused the accumulation of diluvium from the outburst megafloods of the Baige dammed lake at the First Bend area (Shigu town), which is located above the TLG (Figure 4). Typical

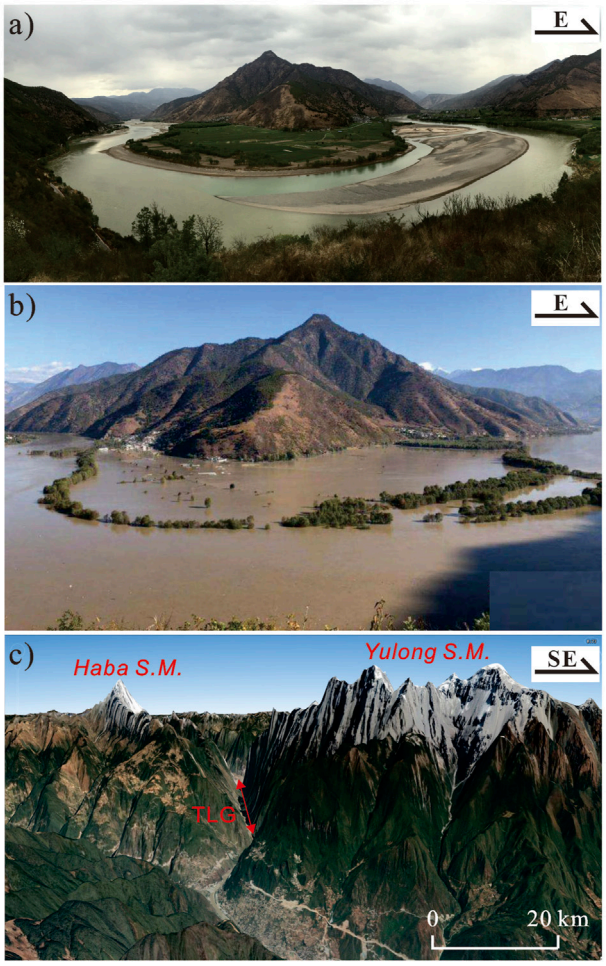

FIGURE 2
(A,B) Photographs of the First Bend of the Yangtze River at the Shigu area. Picture **(A)** was taken on 14 April 2018 and picture **(B)** was taken at 8:45 h on 15 November 2018, when the area was inundated by the outburst flood caused by the broken Baige landslide dam. Picture **(B)** is from the website www.chinanews.com. **(C)** Oblique Google Earth image illustrating that the channel and valley narrowed sharply at the Tiger Leaping Gorge (TLG); terrain contrast is 3.0 times that of the actual. SM: Snow Mountain.

deposits from outburst megafloods that have accumulated in the First Bend area provide ideal materials for the reconstruction of paleo-dammed lakes and their sediments (Figures 2, 4).

3 Methods

3.1 Sample collection

After the flood peaked and subsided, we conducted field investigations to collect samples of accumulated diluvia for ESR studies from three typical sites in the lower reaches of the Baige dammed lake on 15 November 2018. Sampling locations corresponded to deposits generated by the flash flood because strong rainfall was not recorded during that time in the sampling locations, according to reports of the China Meteorological Administration.

In total, 11 samples were collected for ESR signal intensity estimates from three spatially different sections. Samples were collected in stainless steel tubes, and both ends of the tubes were immediately sealed with aluminum foil and taped to prevent light exposure and water loss during transport and storage (Yang et al., 2017). To better understand the grain-size composition of the Baige diluvium, we collected 26 samples from section 4 for grain size analysis at a sampling interval of 10 cm. Detailed information on sampling is provided in Figure 5 and Table 1.

3.2 Protocol for grain size analysis

Grain sizes for all the samples were measured at the Grain Size Measurement Laboratory, Institute of Geology, China Earthquake Administration (IGCEA), using the procedure described by Fan et al. (2006). Chemical pretreatments were performed according to the procedure described by Jiang et al. (2017). Grain size measurements were performed using the Mastersizer 3,000 laser diffraction particle size analyzer.

3.3 Protocol for ESR measurements

3.3.1 Quartz extraction and ESR measurement

Quartz extraction for ESR experiments was performed according to the procedure by Wei et al. (2020). The samples were divided into coarse (100–200 μm) and fine (<100 μm) fractions to investigate the dependence of signal intensity on grain size, according to the procedure described by Voinchet et al. (2015) and Liu et al. (2015). Ten of the 11 aliquots of each sample were irradiated, at doses of 100, 200, 400, 800, 1,200, 1,600, 2000, 3,000, 4,000, and 5,000 Gy. All ESR measurements were executed at the ESR Dating Laboratory, IGCEA, using a BRUKER EPR041XG X-band spectrometer. Ge (g = 1.997) and E_1' (g = 2.001) centers were measured at room temperature (20°C) with a microwave power of 0.01 mW (Figure 6, Toyoda and Ikeya, 1991; Toyoda et al., 2000; Wei et al., 2017). ESR measurements of Al and Ti-Li centers were performed with the spectrometer cooled to 77 K using liquid nitrogen in a finger Dewar. The Al and Ti-Li centers were acquired together with a single spectrum and were realized with a microwave power of 5 mW and modulation amplitude of 0.16 mT. The intensities of the Ti-Li (option A, B, D) and Ti-H centers were measured according to the procedure described by Wei et al. (2020) and Duval and Guilarte (2015) (Figure 6). For each aliquot, readings were obtained at three angles, and the average value was calculated to reduce the difference caused by the anisotropy of quartz. ESR signal intensities were normalized using aliquot weight and receiver gain, and the value of D_e was determined according to the procedure described by Wei et al. (2020).

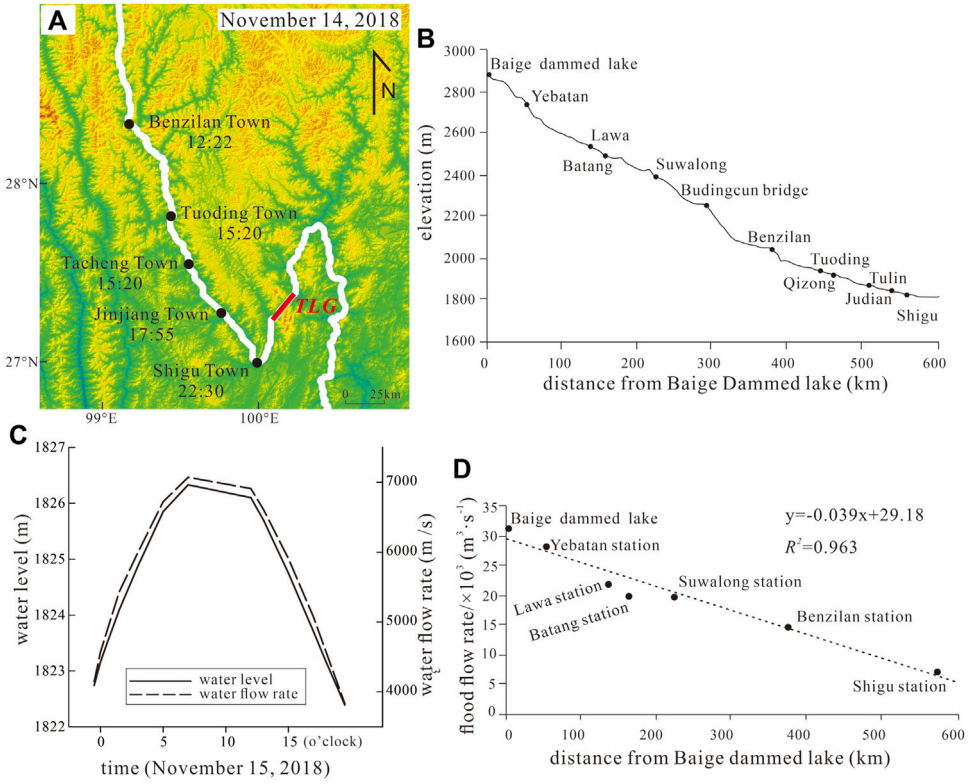

FIGURE 3
(A) Stepped discharge time of diluvium from the Baige dammed lake. **(B)** Riverbed profile of the Jinsha River from the Baige dammed lake to the Shigu area. **(C)** Water level and water flow rate of the Jinsha River in the Shigu area on 15 November 2018 (data from the Bureau of Hydrology, Changjiang Water Resources Commission). Discharge from the Baige dammed lake began at 18:30 h on 13 November 2018 and reached the Shigu area at 22:30 h on 14 November 2018. **(D)** Rate of flood flow from the Baige dammed lake to the Shigu area. **(B,D)** Cited from Su et al. (2021). TLG: Tiger Leaping Gorge.

3.3.2 Bleaching experiment

To evaluate the non-bleachable component and bleaching rate of the Al center, light bleaching of quartz extracted from 11 ESR samples was performed using an SOL 2/500S simulator for 240 h (Wei et al., 2019). The signal intensities for the bleaching rate of ESR centers were calculated according to the procedure described by Voinchet et al. (2015).

4 Results

4.1 Grain size analysis

In this study, grain sizes of < 4 μm, 4–63 μm, and >63 μm were considered to represent clay, silt, and sand fractions, respectively (Folk et al., 1970). Grain parameters were calculated using the method provided by Folk and Ward (1957). Results of grain size analysis are shown in Figure 7 and their comparison with normal deposits in the Yangtze River basin in Table 2.

Figure 7 and Table 2 show that the diluvium is mainly composed of silt (average = 47%) and sand (average = 49%). The frequency distribution curves are characterized by a single peak, which signifies a homogeneous hydrodynamic condition. The probability accumulation curve can be divided into three phases, which represent suspension, saltation, and creeping fractions, respectively. The standard deviation (Sd) varied from 1.37 to 1.21, and the average was 1.52. Skewness (Sk) was 0.21–0.53, with an average of 0.35. Kurtosis granularity (Kg) varied from 0.96 to 1.7, with an average of 1.11. These grain size parameters indicate that the sediments were typical rapid fluvial deposits that had been transported by flow from the Baige dammed lake.

4.2 Residual signal intensities of multiple ESR centers

Quartz Ge centers were not observed, or could not be measured, for all samples presented in the study. However,

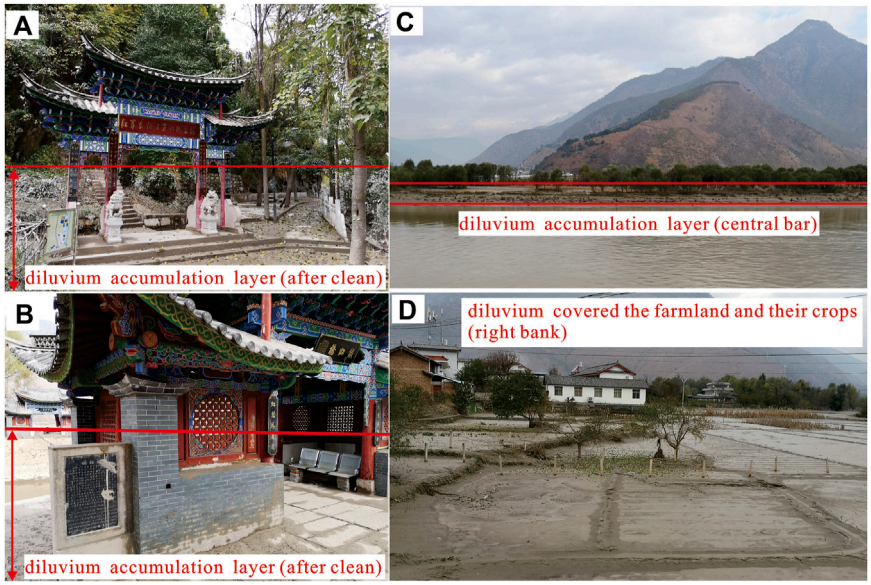

FIGURE 4
Accumulation of diluvium in various locations in the First Bend area (Shigu town) of the Jinsha River. **(A,B)** Diluvium covered the dwellings at the right bank of the Jinsha River; photographs were taken after cleaning. **(C)** Diluvium outcropped at the central bar after the megafloods disappeared. **(D)** Megaflood outburst sediments covered the farmlands and their crops.

the Al, E_1', Ti-H, and Ti-Li centers (options A, B, and D) were measured, and the results are illustrated in Figure 8.

The Al and E_1' centers have the highest residual ESR signal intensities (hereafter referred to as ESR-SI), at 3.8–5 × 10^6 and 2.4–3.4 × 10^6 a.u., respectively. Ti-H centers and Ti-Li centers for option D show the lowest residual ESR-SI, at 1.1–2.3 × 10^5 and 1.2–2.7 × 10^5 a.u., respectively. The Ti-Li centers option and option B show similar residual ESR-SI values, with shifts of 2.0–5.5 × 10^5 and 1.6–5.0 × 10^5 a.u., respectively.

Figure 8 also demonstrates that for the measurement of quartz ESR signal intensity in the same center, the residual ESR-SI of the coarse fractions shows no difference from those of fine fractions, which may be caused by the various provenances of the diluvia and insufficient exposure to sunlight (Voinchet et al., 2015). In conclusion, all observed ESR centers show the same trend of the ESR-SI never reaching zero before burial. Moreover, various samples also show different residual signal intensities within the same center of measurement.

4.3 The Al center bleaching rate and its differences in various grain-size fractions

Figures 8, 9 also show that there is no grain size dependence for natural quartz in the ESR signal intensities of the Al center. However, residual ESR-SI and bleaching rate show a similar trend and vary with the grain size.

The residual ESR-SI of the Al center of quartz was 2.59–2.92 and 2.91–3.35 a.u. in the coarse and fine fractions, respectively. As expected, the fine fractions displayed higher bleaching rates (32–42%, average = 36%) than those of the coarse fractions (20–36%, average = 30%; Figure 9).

Results of previous artificial bleaching experiments showed the non-bleachable part of the Al center to range from 40 to 60% (Voinchet et al., 2003; Lin et al., 2006; Tissoux et al., 2008; Liu and Grün, 2011). Our results indicate that the residual rates of the Al center varied between 66 and 70%, which is higher than those reported by previous studies. Our results indicate that even the bleachable part of the Al center is not "zeroed" by the rapid erosion–transportation–deposition process.

Moreover, our data demonstrate that fine fractions have higher bleaching rates than do coarse fractions (Figures 8, 9). Voinchet et al. (2015) and Liu et al. (2015) attributed the dependence of bleaching rate on grain size to the transportation model, that is, the fraction in suspension is exposed to sunlight for a longer duration during transportation compared to the fraction in saltation. However, our samples were rapidly eroded and accumulated, and their flow was extremely cloudy compared to the samples studied by Voinchet et al. (2015) and Liu et al. (2015). In this situation, the fine and coarse fractions are not exposed to enough sunlight at the same time. Therefore, except for sunlight exposure, the different bleaching rates of Al centers in fine and coarse fractions arise because the coarse quartz is larger and has been trapped deeper compared to fine quartz (Voinchet et al., 2003; Lin et al.,

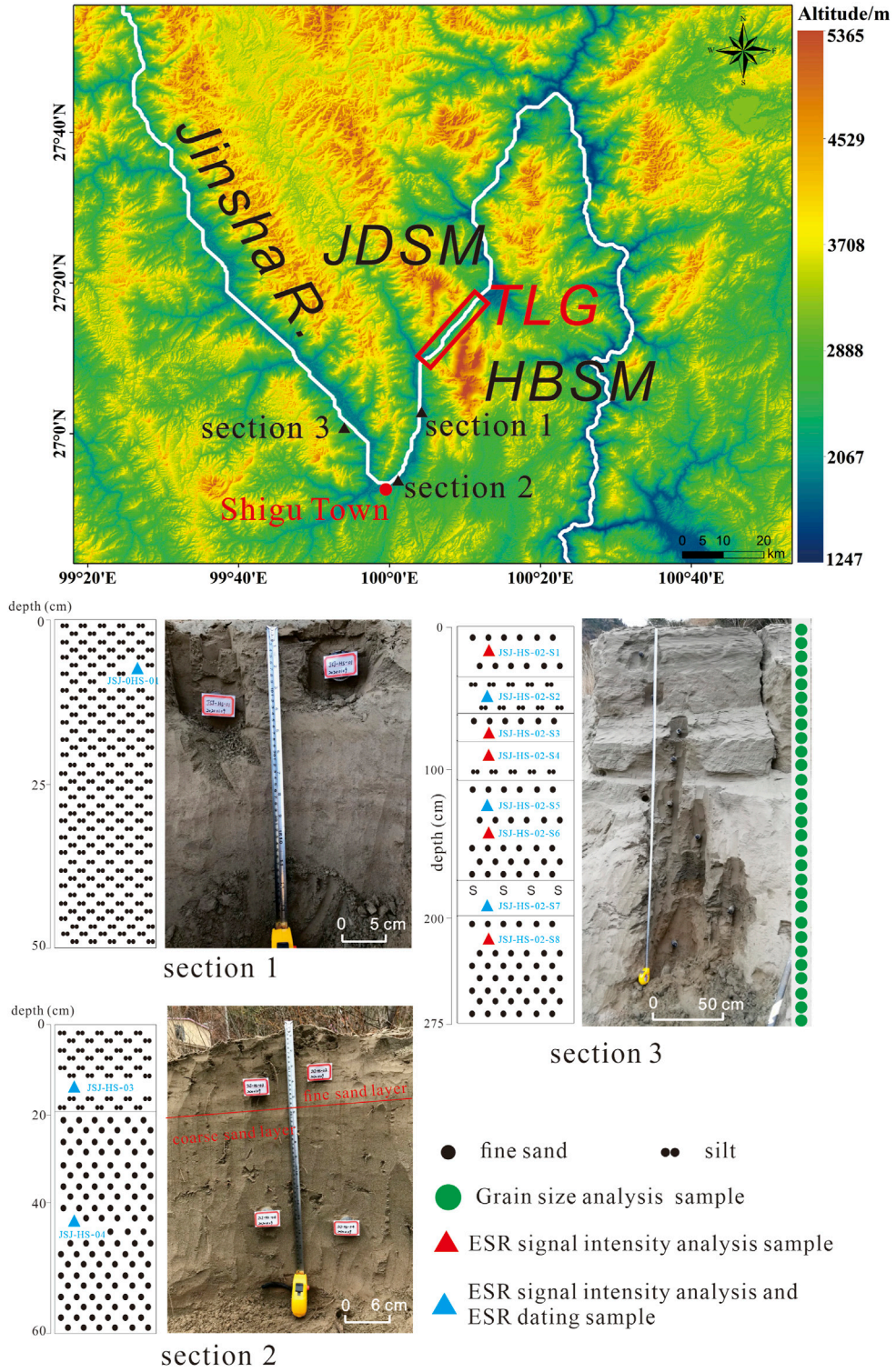

FIGURE 5
Locations and field photos of sampling sections, and their lithological sections. JDSM: Jade Dragon Snow Mountain; HBSM: Haba Snow Mountain; TLG: Tiger Leaping Gorge.

TABLE 1 Details of sampling information for ESR dating and grain size analysis.

Section no.	Location	ESR sample no.	Numbers of samples for grain size analysis
Section 1	27° 03′ 03″ N and 100° 04′ 43″ E; 1820 m	JSJ-HS-01	LD29
Section 2	26° 52′ 09″ N and 99° 57′ 45″ E; 1823 m	JSJ-HS-03	LD27 and LD28
		JSJ-HS-04	
Section 3	26° 54′ 48″ N and 99° 56′ 59″ E; 1827 m	JSJ-HS-02-S1	LD01-LD26
		JSJ-HS-02-S2	
		JSJ-HS-02-S3	
		JSJ-HS-02-S4	
		JSJ-HS-02-S5	
		JSJ-HS-02-S6	
		JSJ-HS-02-S7	
		JSJ-HS-02-S8	

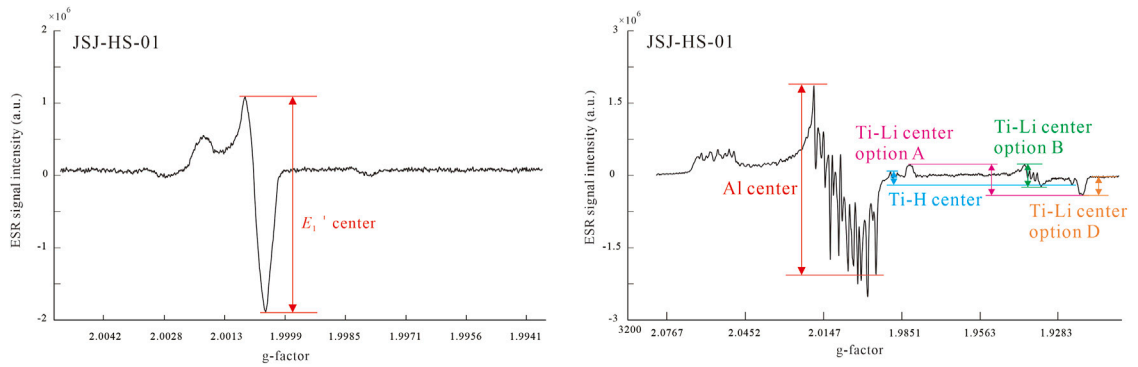

FIGURE 6
ESR spectra of the E_1′ center measured at room temperature for Al and multiple Ti centers measured at a low temperature (77 K) in sample JSJ-HS-01.

2006; Tissoux et al., 2008; Liu and Grün, 2011; Benzid and Timar-Gabor, 2020; Timar-Gabor et al., 2020).

4.4 Comparison of residual ESR signals of multiple Ti centers

Our results demonstrate that various Ti centers show different residual ESR signal intensities (Figure 7). Residual doses of Ti-Li centers (option A) and Ti-Li centers (option B) are twice as large as those of Ti-Li centers (option D) and Ti-H. Duval and Guilarte (2015) demonstrated that options A and D of the Ti-Li center are suitable for accurate ESR dosimetry. It is therefore possible that option D has the lowest ESR residual dose and provides an accurate D_e for the dating of diluvium.

5 Discussion

5.1 Characteristics of the sedimentary structure of outburst megaflood sediment and its comparison with normal Yangtze deposits

Rapids were formed after the barrier dam was destroyed, and they delivered large volumes of water downstream, simultaneously sweeping down sedimentary strata such as the sediments accumulated on high terraces and steep slopes downstream. Mixed sediments were transported by rapids from upstream to downstream and accumulated along the river course, and the bulk (volume) of the diluvium also quickly expanded. As shown in Figure 2, the channel narrowed from approximately 1 km (maximum) to

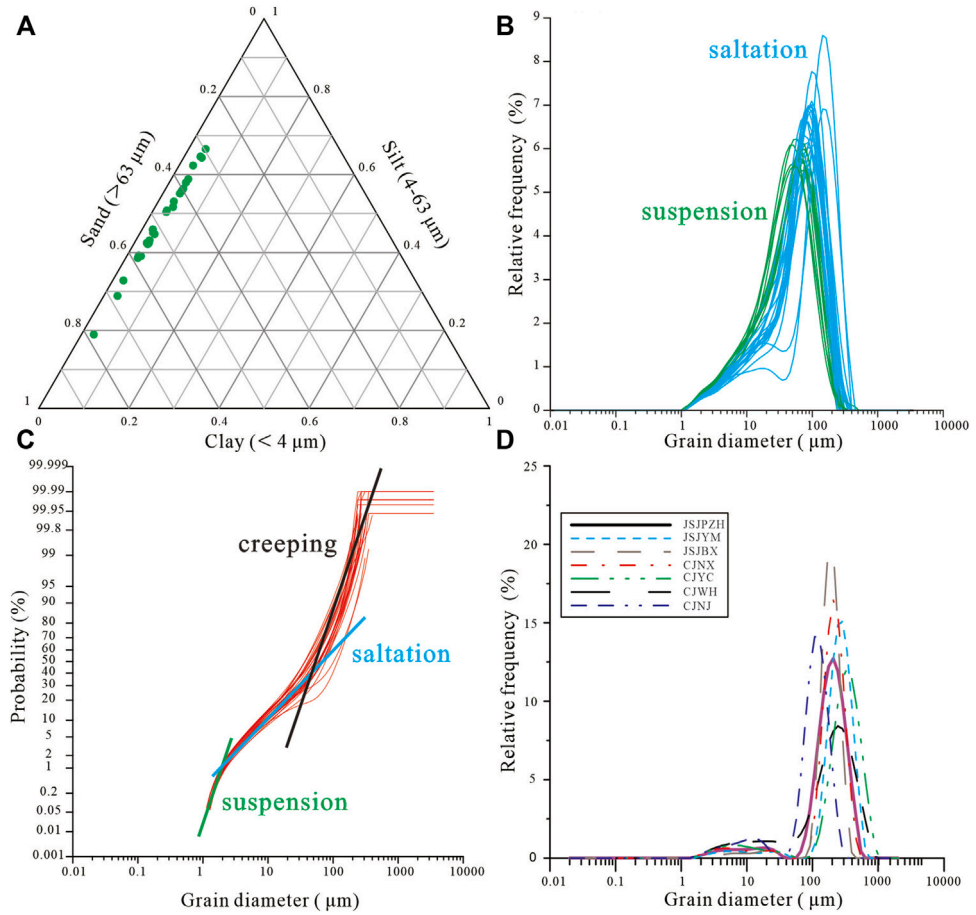

FIGURE 7
Grain size characteristics of diluvium from Baige dammed lake **(A–C)** and other normal Yangtze deposits **(D)**. **(A)** Shepard ternary plot of grain size distribution. **(B,D)** Relative frequency plots of grain size distribution. **(C)** Probability plot of grain size distribution.

TABLE 2 Grain size parameters of diluvia from the Baige dammed lake and normal Yangtze deposits.

	Property	Clay (%)	Silt (%)	Sand (%)	Md (μm)	Mz (μm)	Sd	Sk	kg
Baige dammed lake diluvia	Maximum	4	67	78	133	130	1.81	0.53	1.70
	Minimum	2	19	30	42	48	1.37	0.21	0.96
	Average	3	48	49	66	73	1.52	0.35	1.11
Normal Yangtze deposits	Maximum	2.2	16.9	95	3.1	3.2	1.47	−0.31	2.90
	Minimum	0.2	5	81	1.6	1.7	1.14	−0.48	1.50
	Average	1.7	9.3	89	2.2	2.3	1.27	−0.38	2.24

Note: Results of grain size analyses of normal Yangtze deposits are from Wei (2019, PhD thesis).

less than 100 m (minimum) from the edges of the Baige area to the edges of the TLG (Kong et al., 2009, 2012). The rapids were blocked when they reached the entrance of the narrowed TLG, which was similar to a barrier dam, increasing the levels of rapids and slowing them down. In this case, a short-lived barrier lake formed quickly at the upper reaches of the TLG, which caused the deposition and accumulation of the diluvium at both banks, as shown in Figures 2, 4, 5. Due to

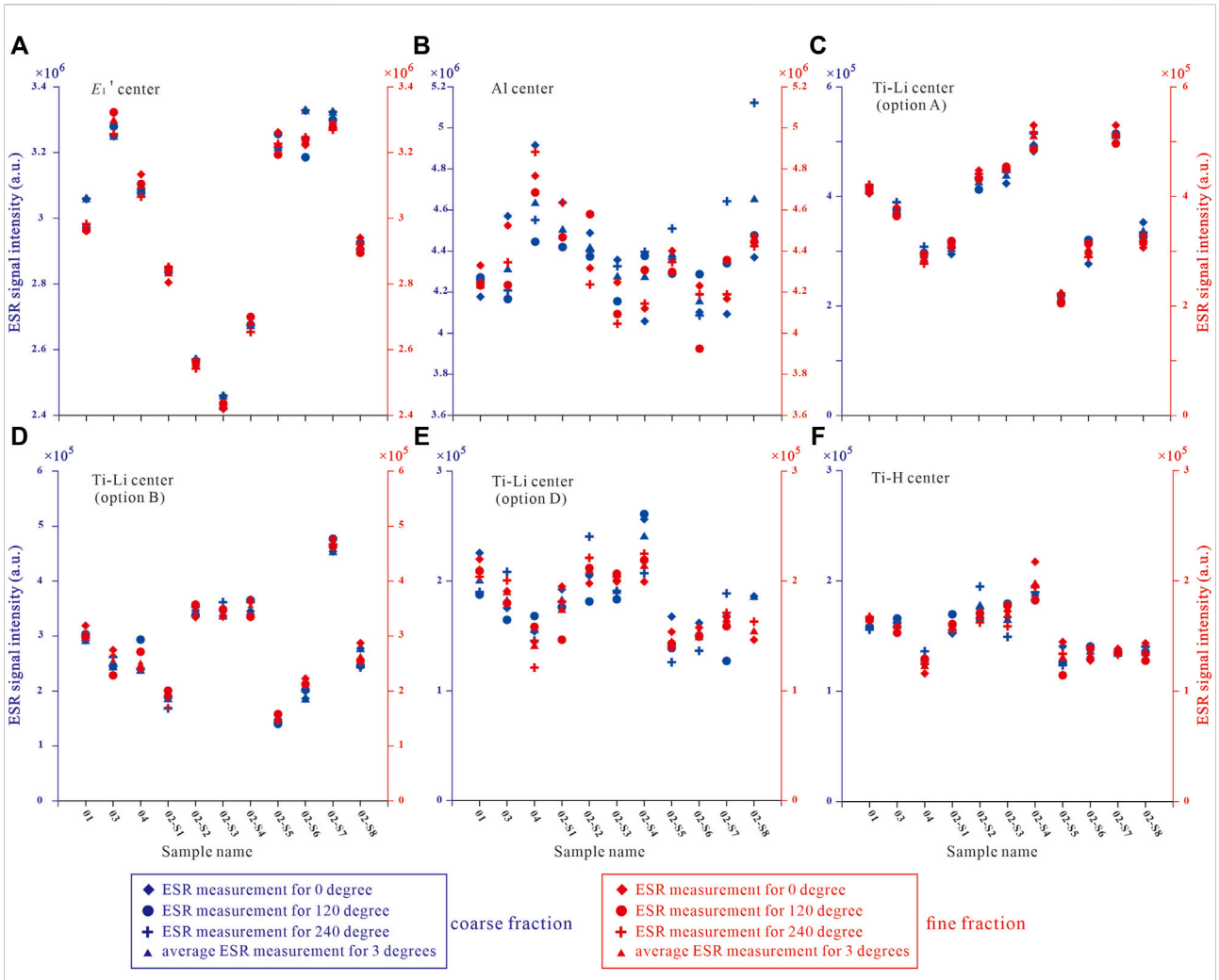

FIGURE 8
Residual signal intensities of multiple ESR centers in coarse and fine fractions of quartz in diluvia of the Baige dammed lake. The coarse and fine quartz residual signal intensities of E1 ' center for **(A)**, Al center for **(B)**, Ti-Li center (option A) for **(C)**, Ti-Li center (option A) for **(D)**, Ti-Li center (option A) for **(E)**, Ti-H center for **(F)**.

the formation and fading of the dammed lake, these diluvia have a finer grain size than those of normal Yangtze deposits, which are similar to lacustrine deposits (Figures 7B,D; Table 2).

In addition to the effects of the dammed lake on hydrodynamic weakening, the upstream rapids did not arrive at the upper reaches of the TLG at the same time, and the level of accumulation increased continuously rather than instantaneously. The diluvium of the Baige dammed lake consequently has good stratification and sorting characteristics (Figures 5, 7, 10), as indicated by measured grain size parameters (Table 2). Furthermore, Figures 5, 10 also show that these megaflood sediments directly covered the bedrocks or previous sedimentary strata, unlike the normal fluvial sediments, which usually show binary structure with coarse lower fractions and fine upper fractions.

5.2 Grain size dependence of residual ESR signal intensities

No marked grain-size dependence of residual signal intensities on multiple ESR centers was observed, as shown in Figure 8. These results differ from those obtained by Voinchet et al. (2015) and Liu et al. (2015), who reported that the lowest residual doses were obtained from quartz grains of 100–200 μm and suggested that these grains were transported in clear water. Their results also showed that the residual doses were small enough to allow for ESR dating of their sediments. However, the phenomenon observed in this study is due to the fact that quartz in the diluvium is mainly transported by extreme turbidity suspension (Voinchet et al., 2015). These materials from the rapids are sourced from various downstream terraces and slopes along the river; they are of old ages and are exposed directly to

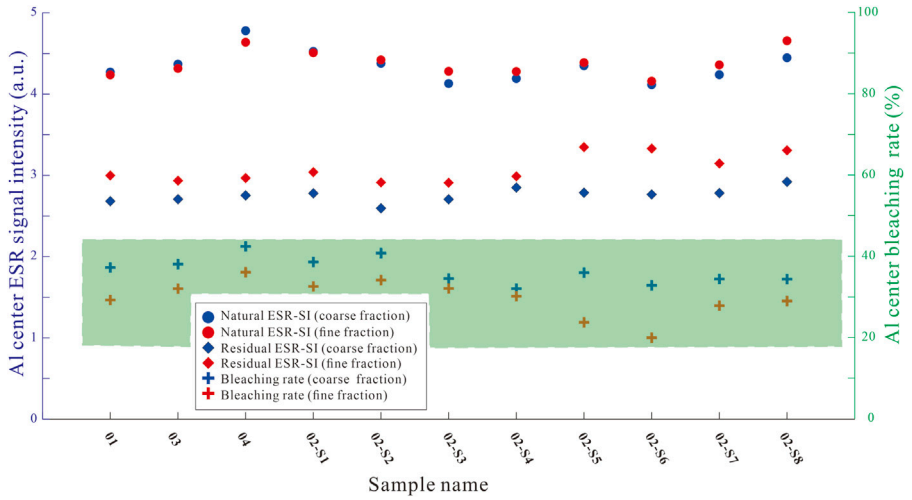

FIGURE 9
Comparison of natural and residual quartz Al center ESR signal intensity (ESR-SI).

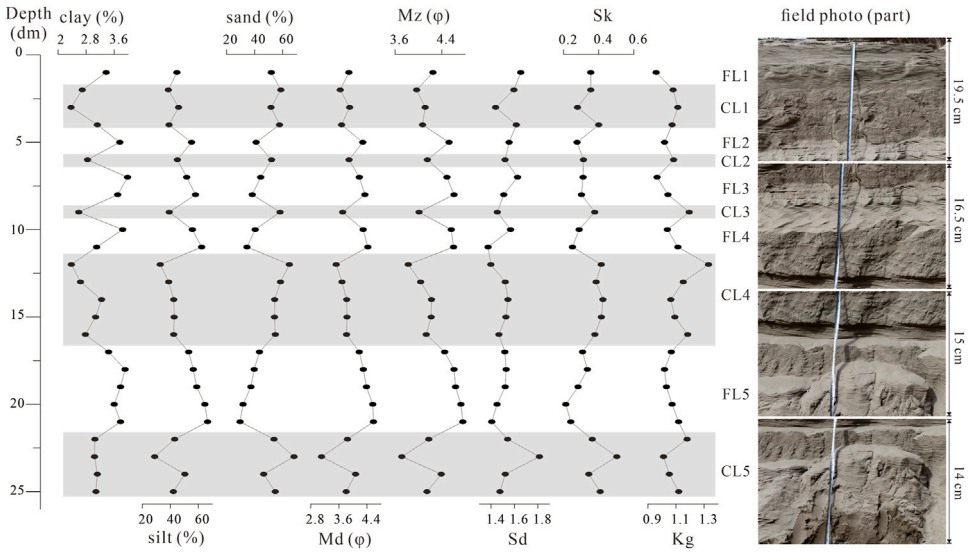

FIGURE 10
Vertical variations of diluvia grain sizes from the analytical results shown in Figure 5 (Section 3). The 250-cm depth section can be classified into five coarse layers (CL1–CL5) and five fine layers (FL1–FL5), which indicate that the diluvium shows good stratification and sorting characteristics in the dammed lake reaches of the canyon areas of large rivers.

light in a mud-flow state either rarely or for a short time. Moreover, these materials carried by the outburst megaflood flow are easy to carry and transport in poor light-exposure conditions. Therefore, ESR residual signal intensities of the diluvium in the Baige dammed lake were not dependent on grain sizes, a finding that is not consistent with previous studies (Liu et al., 2015; Voinchet et al., 2015).

5.3 Differences in residual doses of normal deposits and outburst megaflood sediment

Wei et al. (2020) showed that ESR signals of quartz Ti-Li centers (option A) of the normal present-day fluvial sediments within the Yangtze River Basin could be reset to zero by sunlight

TABLE 3 ESR dating results of diluvia from Baige dammed lake.

Sample no.	U (ppm)	Th (ppm)	K (%)	Water content (%)	Dose rate (Gy/ka)	Equivalent dose (Gy)		Age (ka)
JSJ-HS-01	1.94 ± 0.01	9.58 ± 0.15	1.91 ± 0.01	10 ± 3	2.84 ± 0.07	Ti-Li center	388 ± 83	137 ± 29
						Al center	1,335 ± 366	470 ± 129
JSJ-HS-03	1.86 ± 0.01	9.50 ± 0.15	1.85 ± 0.01	10 ± 3	2.76 ± 0.07	Ti-Li center	332 ± 70	120 ± 25
						Al center	1,010 ± 88	366 ± 32
JSJ-HS-04	1.80 ± 0.01	9.46 ± 0.15	1.71 ± 0.01	10 ± 3	2.58 ± 0.06	Ti-Li center	462 ± 63	179 ± 24
						Al center	1,400 ± 219	543 ± 85
JSJ-HS-02-S2	1.73 ± 0.01	10.7 ± 0.15	1.69 ± 0.01	10 ± 3	2.61 ± 0.06	Ti-Li center	398 ± 31	152 ± 12
						Al center	1,302 ± 305	499 ± 117
JSJ-HS-02-S5	1.84 ± 0.01	11.2 ± 0.15	1.67 ± 0.01	10 ± 3	2.62 ± 0.06	Ti-Li center	283 ± 42	108 ± 16
						Al center	820 ± 168	313 ± 64
JSJ-HS-02-S7	1.72 ± 0.01	11.0 ± 0.15	1.82 ± 0.01	10 ± 3	2.69 ± 0.06	Ti-Li center	317 ± 47	118 ± 17
						Al center	1,356 ± 383	504 ± 142

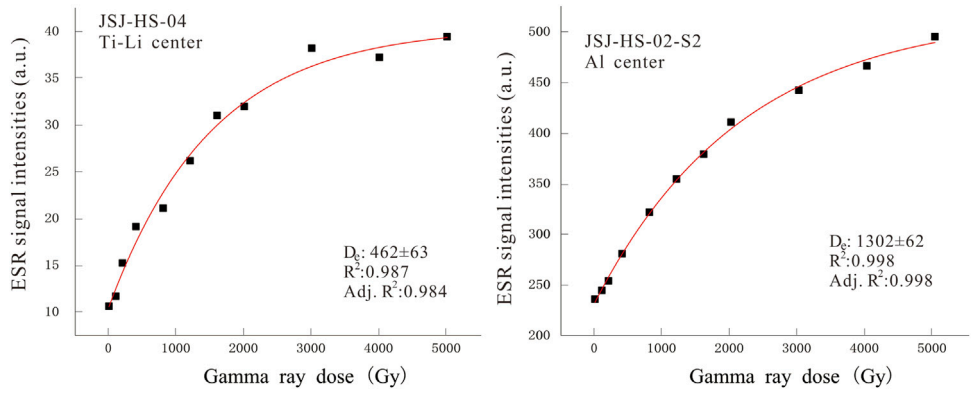

FIGURE 11
Dose response curves of the Ti-Li center (option A) of JSJ-HS-04 and the Al center of JSJ-HS-02-S2.

bleaching after the normal erosion–transportation–deposition cycle. However, this study shows that the high residual ESR signals of Ti-Li centers (options A, B, D) and Al centers in the studied deposits are without efficient sunlight exposure during a rapid transport process with turbid fluvial conditions. Therefore, the good stratification and sorting characteristics of the fluvial sediment indicate that the ESR signals may not completely reset to zero.

Table 3 shows that outburst flood deposits (Baige dammed lake diluvium) in the First Bend area (Shigu town) have large residual doses. The ESR ages of samples indicate that the flood deposits were very poorly bleached, which can be attributed to the fact that sediments were hardly exposed to any sunlight during their transport. The ESR ages obtained from Al centers are always older than those from Ti-Li centers, indicating that the Al center ESR signals were less sensitive to sunlight exposure; this suggests that the Ti-Li center is more sensitive to sunlight bleaching than is the Al center (Figure 11).

As for the E_1' center, Toyoda and Schwarcz (1997) and Toyoda (2015) indicate that the E_1' center is used more in thermal history study than in sediment dating of the quartz, and the observed isotropic signal is unstable even though the intensity increases with gamma ray irradiation. Therefore, applications using the E_1' center for sediment dating remain unclear. Hereafter, Wei et al. (2019) imply that the E_1' center exhibits a rapid increase in the first 16 h, reaches a maximum intensity between 32 h and 230 h, and then slowly decreases to a stable intensity after 400 h, at a level about 2.5 times its normal intensity. These experimental results demonstrate that no new useful indication exists for the possible use of the E_1' center for ESR dating. Thus, the further use of the E_1' center in diluvium dating is discussed in this study.

5.4 Implications for dating of fluvial sediments using ESR signals

Residual signal intensities without efficient sunlight exposure result in an older apparent age of fluvial sediments than the age given by ESR dating (Hu et al., 2010; Zhao et al., 2015). Field investigations show that fluvial sediments usually show good stratification and sorting characteristics; however, various ESR signals of these materials may not be zeroed because of their rapid transportation and accumulation. Particularly in the chronological determination of sequences of the geological profile, when a layer's age is older than the layers below it, with abrupt and inconsistent results in the ESR dating of multiple centers, we can infer the layer to be diluvium, in the absence of other inducements.

Many large international rivers have originated in the Tibetan Plateau and drained through a region with an altitude of 5,000 to 6,000 m above sea level. The large difference in terrain elevation within a limited distance results in strong fluvial erosion, leading to deep, narrow canyons and high mountains. With strong and frequent active fault activities and strong precipitation from the Indian summer monsoon along the Tibetan Plateau, channels of these large rivers are frequently blocked by landslides. The large volume of water discharged from upstream has strong hydrodynamics to carry a large volume of diluvium eroded downstream along the riverbanks. The diluvium is deposited in a flat area with good stratification and sorting characteristics. Therefore, in determining the chronology of the fluvial sediment profile in large river basins, we should attend to layers that show an abrupt age reversal and reconsider their geological and geomorphological implications.

6 Conclusion

In the present study, we investigated quartz residual doses in various ESR signals for diluvium formed by outburst megafloods from the bursting of a dammed lake and deposited in the canyon area of the southeastern Tibetan Plateau. The following conclusions can be drawn based on the results of analyses:

1) Outbursts of large dammed lakes that were blocked by landslides occurred on the Tibetan Plateau, causing outburst megafloods and the accumulation of diluvium, which directly covered the downstream bedrocks and previous sedimentary strata. These megaflood sediments show good stratification and sorting characteristics despite their various provenances because of the diversity of materials swept along the high terraces and slopes downstream.
2) Among the multiple quartz ESR centers observed in this study, the Al, E_1', Ti-H, and Ti-Li centers (options A, B, and D) could be measured. The Ti-H and Ti-Li centers (option D) of diluvium quartz showed the lowest residual dose and indicated a relatively accurate age for rapid fluvial deposits. Ti-Li centers and Al centers, which are commonly used for ESR dating, overestimate by 283 ± 42 ka ~ 462 ± 63 ka and 1,010 ± 88 ka ~ 1,400 ± 219 ka for present outburst megaflood sediment, respectively.
3) In terms of establishing the chronological framework for the fluvial sediment profile, the abrupt reversal of the age of sedimentary layers may be attributed to diluvium deposits. Therefore, whether ESR signal intensities of quartz can be reset to zero or attain steady residual doses before burial cannot be determined by good stratification and sorting characteristics observed during fieldwork.

Data availability statement

The original contributions presented in the study are included in the article/Supplementary Material; further inquiries can be directed to the corresponding author.

Author contributions

CW and GY designed and executed the field investigation and experiment. JD, CL, and HJ analyzed the dataset, while LW also took part in the field investigation. CW, GY, and JD wrote the manuscript. All authors contributed to the article and approved the submitted version.

Funding

This work was supported by the National Natural Science Foundation of China (Grant Nos. 41772185 and 42002203) and the National Nonprofit Fundamental Research Grant of China, Institute of Geology, China, Earthquake Administration (Grant Nos. IGCEA2226 and IGCEA1715).

Conflict of interest

The authors declare that the research was conducted in the absence of any commercial or financial relationships that could be construed as a potential conflict of interest.

The handling editor declared a past co-authorship with the authors CW, GY, and CL.

Publisher's note

References

Ambraseys, N. N., and Douglas, J. (2004). Magnitude calibration of north Indian earthquakes. *Geophys. J. Int.* 159, 165–206. doi:10.1111/j.1365-246X.2004.02323.x

Bartz, M., Duval, M., Brill, D., Zander, A., King, G. E., Rhein, A., et al. (2020). Testing the potential of K-feldspar pIR-IRSL and quartz ESR for dating coastal alluvial fan complexes in arid environments. *Quat. Int.* 556, 124–143. doi:10.1016/j.quaint.2020.03.037

Benzid, K., and Timar-Gabor, A. (2020). Phenomenological model of aluminium-hole ([AlO4/h+]0) defect formation in sedimentary quartz upon room temperature irradiation: Electron spin resonance (ESR) study. *Radiat. Meas.* 130, 106187. doi:10.1016/j.radmeas.2019.106187

Carrivick, J. L., Jones, R., and Keevil, G. (2011). Experimental insights on geomorphological processes within dam break outburst floods. *J. Hydrology* 408, 153–163. doi:10.1016/j.jhydrol.2011.07.037

Cunningham, A. C., Evans, M., and Knight, J. (2015). Quantifying bleaching for zero-age fluvial sediment: A bayesian approach. *Radiat. Meas.* 81, 55–61. doi:10.1016/j.radmeas.2015.04.007

Ding, Y. Y., Zhang, X. J., He, Z. X., Lu, C. Y., and Bao, S. Y. (2021). Sedimentary environment of a dammed lake buried in the modern riverbed of the Yalong River during the Last Glacial Maximum and its implication for fluvial geomorphic evolution. *Geomorphology* 378, 107588. doi:10.1016/j.geomorph.2020.107588

Dong, G. H., Zhang, F. Y., Liu, F. W., Zhang, Ds. J., Zhou, A. F., Yang, Y. S., et al. (2018). Multiple evidences indicate no relationship between prehistoric disasters in Lajia site and outburst flood in upper Yellow River valley, China. *Sci. China Earth Sci.* 61, 441–449. doi:10.1007/s11430-017-9079-3

Duval, M., Arnold, L. J., Guilarte, V., Demuro, M., Santonja, M., and Pérez-González, A. (2017). Electron spin resonance dating of optically bleached quartz grains from the Middle Palaeolithic site of Cuesta de la Bajada (Spain) using the multiple centres approach. *Quat. Geochronol.* 37, 82–96. doi:10.1016/j.quageo.2016.09.006

Duval, M., and Guilarte, V. (2015). ESR dosimetry of optically bleached quartz grains extracted from Plio-Quaternary sediment: Evaluating some key aspects of the ESR signals associated to the Ti-centers. *Radiat. Meas.* 78, 28–41. doi:10.1016/j.radmeas.2014.10.002

Fan, M., Song, C., Dettman, D. L., Fang, X., and Xu, X. (2006). Intensification of the asian winter monsoon after 7.4 ma: Grain-size evidence from the linxia basin, northeastern Tibetan plateau, 13.1 ma to 4.3 ma. *Earth Planet. Sci. Lett.* 248, 186–197. doi:10.1016/j.epsl.2006.05.025

Folk, R. L., Andrews, P. B., and Lewis, D. W. (1970). Detrital sedimentary rock classification and nomenclature for use in New Zealand. *N. Z. J. Geol. Geophys.* 13, 937–968. doi:10.1080/00288306.1970.10418211

Folk, R. L., and Ward, W. C. (1957). Brazos River bar [Texas]; a study in the significance of grain size parameters. *J. Sediment. Res.* 27, 3–26. doi:10.1306/74D70646-2B21-11D7-8648000102C1865D

Gao, L., Yin, G. M., Liu, C. R., Bahain, J. J., Lin, M., and Li, J. P. (2009). Natural sunlight bleaching of the ESR titanium center in quartz. *Radiat. Meas.* 44, 501–504. doi:10.1016/j.radmeas.2009.03.033

Gliganic, L. A., Cohen, T. J., Meyer, M., and Molenaar, A. (2017). Variations in luminescence properties of quartz and feldspar from modern fluvial sediments in three rivers. *Quat. Geochronol.* 41, 70–82. doi:10.1016/j.quageo.2017.06.005

Grün, R. (1989). ESR dating for the early Earth. *Nature* 338, 543–544. doi:10.1038/338543a0

Guo, X. Y., Guo, Q., and Feng, Z. K. (2021). Detecting the vegetation change related to the creep of 2018 Baige landslide in Jinsha River, SE tibet using SPOT data. *Front. Earth Sci.* 9, 706998. doi:10.3389/feart.2021.706998

Hu, G., Zhang, J.-F., Qiu, W.-L., and Zhou, L.-P. (2010). Residual OSL signals in modern fluvial sediments from the Yellow River (HuangHe) and the implications for dating young sediments. *Quat. Geochronol.* 5, 187–193. doi:10.1016/j.quageo.2009.05.003

Jiang, H., Zhong, N., Li, Y., Ma, X., Xu, H., Shi, W., et al. (2017). A continuous 13.3-ka record of seismogenic dust events in lacustrine sediments in the eastern Tibetan Plateau. *Sci. Rep.* 7, 15686. doi:10.1038/s41598-017-16027-8

Kong, P., Na, C., Fink, D., Zhao, X., and Xiao, W. (2009). Moraine dam related to late Quaternary glaciation in the Yulong Mountains, southwest China, and impacts on the Jinsha River. *Quat. Sci. Rev.* 28, 3224–3235. doi:10.1016/j.quascirev.2009.08.005

Kong, P., Zheng, Y., and Caffee, M. W. (2012). Provenance and time constraints on the formation of the first bend of the Yangtze River. *Geochem. Geophys. Geosyst.* 13 (6), a–n. doi:10.1029/2012GC004140

Li, L., Chen, J., Hedding, D. W., Fu, Y., Ye, M., and Li, G. (2020). Uranium isotopic constraints on the nature of the prehistoric flood at the Lajia site, China. *China. Geol.* 48, 15–18. doi:10.1130/G46306.1

Li, N., Wang, R., Liu, Y., Du, K., Chen, J., and Deng, Y. (2014). Robust river boundaries extraction of dammed lakes in mountain areas after Wenchuan Earthquake from high resolution SAR images combining local connectivity and ACM. *ISPRS J. Photogrammetry Remote Sens.* 94, 91–101. doi:10.1016/j.isprsjprs.2014.04.020

Lin, M., Yin, G., Ding, Y., Cui, Y., Chen, K., Wu, C., et al. (2006). Reliability study on ESR dating of the aluminum center in quartz. *Radiat. Meas.* 41, 1045–1049. doi:10.1016/j.radmeas.2006.05.019

Liu, C. R., and Grün, R. (2011). Fluvio-mechanical resetting of the Al and Ti centres in quartz. *Radiat. Meas.* 46, 1038–1042. doi:10.1016/j.radmeas.2011.06.076

Liu, C. R., Yin, G. M., and Han, F. (2015). Effects of grain size on quartz ESR dating of Ti-Li center in fluvial and lacustrine sediments. *Quat. Geochronol.* 30, 513–518. doi:10.1016/j.quageo.2015.02.007

Liu, W. M., Carling, P. A., Hu, K. H., Wang, H., Zhou, Z., Zhou, L. P., et al. (2019). Outburst floods in China: A review. *Earth-Science Rev.* 197, 102895. doi:10.1016/j.earscirev.2019.102895

Moreno, D., Falguères, C., Pérez-González, A., Duval, M., Voinchet, P., Benito-Calvo, A., et al. (2012). ESR chronology of alluvial deposits in the arlanzón valley (atapuerca, Spain): Contemporaneity with atapuerca gran dolina site. *Quat. Geochronol.* 10, 418–423. doi:10.1016/j.quageo.2012.04.018

Richter, M., and Tsukamoto, S. (2022). Investigation of quartz electron spin resonance residual signals in the last glacial and early Holocene fluvial deposits from the Lower Rhine. *Geochronology* 4, 55–63. doi:10.5194/gchron-4-55-2022

Rink, W. J. (1997). Electron spin resonance (ESR) dating and ESR applications in quaternary science and archaeometry. *Radiat. Meas.* 27, 975–1025. doi:10.1016/S1350-4487(97)00219-9

Su, H., Shi, Z. T., Dong, M., Ye, L. T. Y., and Ye, L. (2021). The geomorphic process and sedimentary characteristics of the "11·3" Baige Dammed Lake outburst flood event in the upper reaches of the Jinsha River from Benzilan to Shihku. *Earth Sci. Front.* 28 (2), 202–210. doi:10.13745/j.esf.sf.2020.9.19

Timar-Gabor, A., Chruścińska, A., Benzid, K., Fitzsimmons, K. E., Begy, R., and Bailey, M. (2020). Bleaching studies on Al-hole ([AlO4/h]0) electron spin resonance (ESR) signal in sedimentary quartz. *Radiat. Meas.* 130, 106221. doi:10.1016/j.radmeas.2019.106221

Tissoux, H., Toyoda, S., Falguères, C., Voinchet, P., Takada, M., Bahain, J.-J., et al. (2008). ESR dating of sedimentary quartz from two pleistocene deposits using Al and Ti-centers. *Geochronometria.* 30, 23–31. doi:10.2478/v10003-008-0004-y

Toyoda, S., and Ikeya, M. (1991). Thermal stabilities of paramagnetic defect and impurity centers in quartz: Basis for ESR dating of thermal history. *Geochem. J.* 25, 437–445. doi:10.2343/geochemj.25.437

Toyoda, S. (2015). Paramagnetic lattice defects in quartz for applications to ESR dating. *Quat. Geochronol.* 30, 498–505. doi:10.1016/j.quageo.2015.05.010

Toyoda, S., and Schwarcz, H. P. (1997). The hazard of the counterfeit E_1' signal in quartz to the ESR dating of fault movements. *Quat. Sci. Rev.* 16 (3-5), 483–486. doi:10.1016/S0277-3791(96)00088-1

Toyoda, S., Voinchet, P., Falguères, C., Dolo, J. M., and Laurent, M. (2000). Bleaching of ESR signals by the sunlight: A laboratory experiment for establishing the ESR dating of sediments. *Appl. Radiat. Isotopes* 52, 1357–1362. doi:10.1016/S0969-8043(00)00095-6

Tsukamoto, S., Porat, N., and Ankjærgaard, C. (2017). Dose recovery and residual dose of quartz ESR signals using modern sediments: Implications for single aliquot ESR dating. *Radiat. Meas.* 106, 472–476. doi:10.1016/j.radmeas.2017.02.010

Voinchet, P., Falguères, C., Laurent, M., Toyoda, S., Bahain, J. J., and Dolo, J. M. (2003). Artificial optical bleaching of the Aluminium center in quartz implications to ESR dating of sediments. *Quat. Sci. Rev.* 22, 1335–1338. doi:10.1016/S0277-3791(03)00062-3

Voinchet, P., Falguères, C., Tissoux, H., Bahain, J.-J., Despriée, J., and Pirouelle, F. (2007). ESR dating of fluvial quartz: Estimate of the minimal distance transport required for getting a maximum optical bleaching. *Quat. Geochronol.* 2, 363–366. doi:10.1016/j.quageo.2006.04.010

Voinchet, P., Pereira, A., Nomade, S., Falguères, C., Bidditu, I., Piperno, M., et al. (2020). ESR dating applied to optically bleached quartz - a comparison with 40Ar/39Ar chronologies on Italian Middle Pleistocene sequences. *Quat. Int.* 556, 113–123. doi:10.1016/j.quaint.2020.03.012

Voinchet, P., Toyoda, S., Falguères, C., Hernandez, M., Tissoux, H., Moreno, D., et al. (2015). Evaluation of ESR residual dose in quartz modern samples, an

investigation on environmental dependence. *Quat. Geochronol.* 30, 506–512. doi:10.1016/j.quageo.2015.02.017

Voinchet, P., Yin, G., Falguères, C., Liu, C., Han, F., Sun, X., et al. (2019). Dating of the stepped quaternary fluvial terrace system of the Yellow River by electron spin resonance (ESR). *Quat. Geochronol.* 49, 278–282. doi:10.1016/j.quageo.2018.08.001

Wang, H., Tong, K., Hu, G., Wang, P., Li, D., Huang, J., et al. (2021). Dam and megafloods at the first bend of the Yangtze River since the last glacial maximum. *Geomorphology* 373, 107491. doi:10.1016/j.geomorph.2020.107491

Wang, L. C., Wen, M. S., Feng, Z., Sun, W. F., Wei, Y. J., Li, J. F., et al. (2019). Researches on the Baige landslide at jinshajiang river, tibet, China. *Chin. J. Geol. Hazard Control* 30 (01), 1–9. doi:10.16031/j.cnki.issn.1003-8035.2019.01.01

Wei, C. Y., Li, C. R., Liu, W., Li, Z., Zhang, H., Zhang, J., et al. (2017). Nature ESR signals of quartz E_1' center shed new light on river sediments provenance: A case study in southeast margin of the tibet plateau. *Quat. Int.* 454, 38–44. doi:10.1016/j.quaint.2017.08.044

Wei, C. Y., Liu, C. R., Li, C. A., Leng, Y. H., Li, W. P., Yin, G. M., et al. (2018). Bleaching characteristics of quartz electron spin resonance (ESR) signals of multiple Ti-Li centers: Implication for ESR dating. *J. Earth Env.* 9, 607–613.

Wei, C. Y., Liu, C. R., Li, C. A., Yin, G. M., Zhang, Y. F., Li, W. P., et al. (2019). Application of long time artificial optical bleaching of the E1' centre to sediment ESR dating. *Geochronometria* 46 (1), 79–86. doi:10.1515/geochr-2015-0106

Wei, C. Y. (2019). Multiple ESR center signals and crystallinity index of quartz: Shed new light on Yangtze River sediments provenance tracing. PhD Thesis, 67–99.

Wei, C. Y., Voinchet, P., Zhang, Y., Bahain, J. J., Liu, C., Kang, C., et al. (2020). Chronology and provenance of the yichang gravel layer deposits in the jianghan basin, middle Yangtze River valley, China: Implications for the timing of channelization of the three gorges valley. *Quat. Int.* 550, 39–54. doi:10.1016/j.quaint.2020.03.020

Wu, Q., Zhao, Z., Liu, L., Granger, D. E., Wang, H., Cohen, D. J., et al. (2016). Outburst flood at 1920 BCE supports historicity of China's Great Flood and the Xia dynasty. *Science* 353, 579–582. doi:10.1126/science.aaf0842

Zhao, Q., Thomsen, K. J., Murray, A. S., Wei, M., Pan, B., Song, B., et al. (2015). Testing the use of OSL from quartz grains for dating debris flows in Miyun, northeast Beijing, China. *Quat. Geochronol.* 30, 320–327. doi:10.1016/j.quageo.2015.03.007